Sustainable Structures
ISSN: 2789-3111 (Print); ISSN: 2789-312X (Online)
http://www.sustain-dpl.com/journal/sust
DOI: 10.54113/j.sust.2025.000076

ORIGINAL ARTICLE

Experimental research and damage analysis on the seismic behavior of ESJ-strengthened seismic-damaged RACFRST columns

Sheng Peng[a,b], Huangkai Sun[a], Dongping Wu[a], Xianqi Xie[c], Ben Mou[d,e,*]

[a]Institute of High Performance Engineering Structure, Wuhan University of Science and Technology, Wuhan 430065, China
[b]School of Civil Engineering, Wuhan University, Wuhan 430072, China
[c]State Key Laboratory of Precision Blasting, Jianghan University, Wuhan 430056, China
[d]School of Civil Engineering, Qingdao University of Technology, Qingdao 266033, China
[e]Department of Civil Engineering, The University of Hong Kong, Hong Kong
[*]Corresponding Author: Ben Mou. E-mail address: mouben@qut.edu.cn (B. Mou)

Abstract: This study examines the seismic response characteristics of pre-damaged recycled-aggregate concrete-encased rectangular steel tube (RACFRST) columns. Four column prototypes underwent cyclic loading experiments to assess the rehabilitation effectiveness of enveloped steel jackets (ESJ) on seismically compromised members. Comprehensive analysis of hysteresis characteristics, rigidity deterioration patterns, strength degradation trends, energy dissipation mechanisms, deformation ductility, and strain distribution was performed using experimental data. A dual-parameter seismic damage evaluation framework was subsequently developed and validated through experimental measurements. Findings revealed that ESJ-retrofitted specimens demonstrated 23-37% enhancement in load-bearing capacity, 18-29% improvement in initial stiffness, and 32-45% increase in cumulative energy dissipation compared to reference specimens. The efficiency of rehabilitation demonstrated a negative correlation with prior damage severity, resulting in a 19% decline in efficacy as the initial damage index rose from 0.3 to 0.6. The proposed damage assessment model yielded indices ranging between 0.92-1.08 for retrofitted components, demonstrating strong correlation with experimental observations. This validated methodology enables quantitative seismic performance evaluation for ESJ-strengthened RACFRST structural elements in post-earthquake rehabilitation scenarios.

Keywords: Recycled-aggregate concrete-filled rectangular steel tube (RACFRST), seismic-damaged, seismic damage model, enveloped steel jackets (ESJ)

1. Introduction

As urbanization and reconstruction progress in China, significant amounts of waste concrete are produced, contributing to environmental pollution and resource depletion. A promising solution to this issue is the extraction of recycled aggregate concrete (RAC) from waste concrete to substitute natural aggregate [1]. Utilizing recycled concrete aggregate (RCA) not only diminishes the need for natural sand extraction, conserving resources, but also mitigates environmental harm [2-4]. Nonetheless, the presence of old mortar in RCA influences its geometric properties, impacting the compressive and tensile characteristics of RAC [5]. Moreover, micro-cracks formed during the crushing process

Received: 1 December 2024; Received in revised form: 16 February 2025; Accepted: 2 May 2025

introduce flaws in RCA, including diminished compressive strength [6-8], inferior ductility [9], decreased workability and elastic modulus [10-12], and increased shrinkage and creep [13-14]. These limitations restrict the use of RAC in structural engineering applications.

RACFST effectively addresses the detrimental effects of recycled aggregate on concrete's mechanical performance while combining the benefits of concrete-filled steel tubes, including superior capacity and seismic resilience, thereby expanding the potential applications of RAC in construction [15-16]. As critical structural elements, RACFRST columns serve essential load-bearing roles in buildings [17]. Their seismic behavior and failure mechanisms closely resemble those of conventional CFST columns, making them viable for high-rise construction due to their structural similarities [18-19].

The capacity of recycled-aggregate concrete-filled steel tube (RACFST) columns generally diminishes as the substitution rate of RCA increases, primarily due to inherent defects in RCA, which accelerate the onset of local buckling in the specimens. However, these mechanical deficiencies can be effectively mitigated by incorporating materials such as fibers or geopolymers into the RAC mixture [20-22]. Wang et al. [23] conducted axial load tests on 39 RACFST columns. Yang et al. [24] investigated the structural behavior of slender rectangular RACFST columns under eccentric compression, documenting their failure mechanisms and load-bearing characteristics. Chen et al. [25] employed artificial neural networks, genetic expression programming, and multiple linear regression to predict the compressive strength of RACFST columns, which provided valuable insights for the broader adoption of RACFST. Yang et al. [26] explored the effects of RCA strength and diameter-to-thickness ratios, finding that RACFST columns could achieve comparable failure modes, ductility, stiffness, and energy dissipation to conventional CFST columns. Luo et al. [27] performed cyclic loading tests on nine RACFST columns, creating a numerical model to evaluate the impact of RCA substitution rates, steel content, axial compression ratios, and diameter-to-thickness ratios. Their results indicated that compression-bending failure was the dominant mode, with axial compression ratios and steel content having significant effects, while RCA substitution rates had minimal influence. Dong et al. [28] studied high-strength RACFST columns, focusing on RCA replacement ratios, shear-span ratios, and axial compression ratios. They observed that failure modes were similar to CFST columns, with load-bearing capacity and ductility largely unaffected by RCA replacement ratios but significantly influenced by shear-span and axial compression ratios.

Common seismic strengthening techniques include section enlargement, carbon fiber-reinforced polymer (CFRP) sheets, buckling-restrained braces, and external steel jacketing (ESJ) [29-32]. While section enlargement and buckling-restrained braces offer effective reinforcement, they often require time-consuming modifications to structural dimensions. CFRP and ESJ methods preserve the original dimensions but differ in effectiveness; CFRP struggles to enhance ultimate load-bearing capacity, whereas ESJ improves both load-bearing capacity and ductility. Abdulrahman Salah et al. [33] compared connected and disconnected steel sleeves, finding that connected sleeves significantly enhanced load-bearing capacity. Rawaa Saadi Ibrahim et al. [34] noted that steel angles increased axial load capacity, while steel strips provided lateral confinement, with ESJ improving seismic stability and reducing strength degradation. Liu et al. [35] studied dry-type steel jackets. Kwan et al. [36] and Lai et al. [37] proposed a theoretical model for circular steel jackets, demonstrating their ability to prevent steel-concrete separation and enhance ductility in plastic hinge zones. Zhang et al. [38] addressed stress lag in steel jackets by using steel hoops, which improved shear capacity and altered failure modes. Zha et al. [39] found that ESJ significantly increased initial stiffness and ultimate load-bearing capacity, especially when jacket thickness matched the steel tube wall thickness. Xu et al. [40] simulated earthquake damage, repaired CFST columns, and tested them under cyclic loading, showing that ESJ effectively restored seismic performance, with damage levels influencing reinforcement outcomes. Despite these advancements, the seismic performance evolution and damage modeling of ESJ-strengthened RACFRST columns, considering both RCA defects and pre-existing seismic damage, remain underexplored and warrant further investigation.

This study examines the seismic behavior of ESJ-strengthened RACFRST columns. The research aims to: (1) evaluate the seismic performance of ESJ-strengthened RACFRST columns and the feasibility of the ESJ method, and (2) develop a two-parameter seismic damage model to elucidate the seismic damage behavior of these columns.

2. Experimental design

2.1. Specimen

Four 1/2-scale RACFRST columns were designed and fabricated for testing. The frame columns featured an exposed base, with stiffening rib plates added to the bottom plate for reinforcement. The steel tubes had a steel ratio of 8.5% for the section. The RAC was prepared according to the specified mix ratio. After pouring, the specimens were cured in the laboratory environment for 28 days. **Figure 1(a)** illustrates the detailed configuration of the test specimens. Based on the code [41], the design flexural capacity was calculated using Eqs. (1) to (3), yielding a value of 56.4 kN·m.

$$M_u = \gamma_m W_{sc} f_{sc} \tag{1}$$

$$W_{sc} = \frac{\pi r_0^3}{4} \tag{2}$$

$$r_m = \left(1 - 0.5\psi\right)\left(-0.483\theta + 1.926\sqrt{\theta}\right) \tag{3}$$

where, γ_m is the plastic development coefficient, W_{sc} is the section modulus of flexural member, f_{sc} is the design value of compressive strength, r_0 is theradius of equivalent circle, ψ is the void ratio, solid components take 0, θ is the hoop coefficient.

The experimental axial compression ratio is obtained by Eq (4), the calculated value is 0.26 [42].

$$n = \frac{N}{f_c \times A_c + f_y \times A_s} \tag{4}$$

where, N is the actual axial load, A_s and A_c are the cross-sectional areas of the steel tube and the filled-in RAC, respectively, f_c is the cubic compressive strengths of the recycled aggregate concrete, f_y is the yield strength of the steel tube.

Artificial simulation of seismic damage serves as the foundation for experimental studies. In accordance with the Code for Seismic Design of Buildings (GB 50011-2010) [43], the interlayer displacement angle was selected as the control parameter for different damage states. Specifically, angles of 1/100 and 1/50 were used to represent moderate and severe damage, respectively. By multiplying these angles by the column's effective height (L = 1200 mm), the corresponding lateral drifts were calculated as 12 mm for moderate pre-damage and 24 mm for severe pre-damage. Based on the Standard for Design of Steel Structures (GB 50017-2017) [44], the height of the strengthening zone was set to 660 mm, ensuring it was at least 2.5 times the column width. The ESJ method was chosen for reinforcement due to its simplicity, adaptability, and ability to enhance structural load-bearing capacity, stiffness, and ductility [45].

The ESJ was first welded to the base plate of the frame column to ensure integrated load transfer [46]. Sealant was then applied to fill gaps between batten plates, followed by the addition of WJS structural adhesive, which was cured for approximately seven days. A detailed illustration of the strengthened specimen is provided in **Fig. 1(b)**.

Table 1. Parameters of specimens

Specimen	Number	Damage degree	Displacement angle	Strengthened level
SEJS-0	1	Undamaged	-	No
SEJS-1	1	Undamaged	-	Yes
SEJS-2	1	Moderate damaged	1/100	Yes
SEJS-3	1	Severe damaged	1/50	Yes

The test variables included pre-damage levels (no damage, moderate damage, and severe damage) and the application of ESJ (with or without). The specimens were labeled as SEJS-0, SEJS-1, SEJS-2, and SEJS-3. SEJS-0 served as the undamaged and unstrengthened control specimen, while SEJS-1 was strengthened without prior damage. SEJS-2 and SEJS-3 were subjected to 12 mm and 24 mm displacement to simulate moderate and severe damage, respectively, before being reinforced with ESJ. **Table 1** summarizes the specimen parameters.

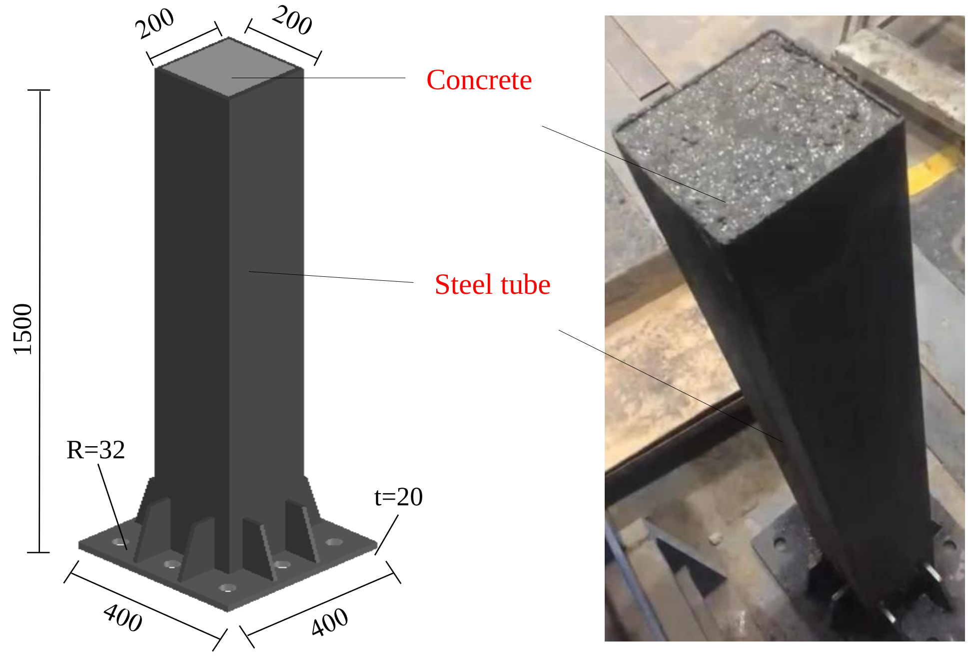

(a) The contrast specimen

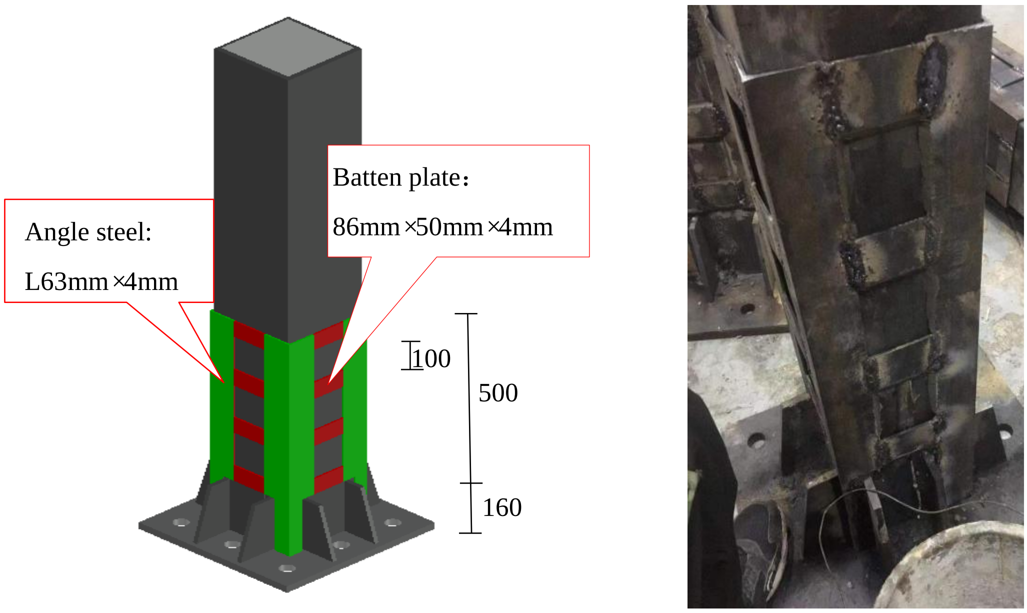

(b) The ESJ-strengthened specimen

Fig. 1. Specimen construction. (Unit: mm)

2.2. Material properties

When the replacement rate of RCA reached 50%, the mechanical properties of RACFRST columns exhibited the most pronounced changes [47]. Consequently, this study adopted a 50% replacement rate, meaning half of the coarse aggregate's mass was substituted with RCA. **Table 2** presents the physical characteristics of the RCA. In line with the Specification for Mix Proportion Design of Ordinary Concrete (JGJ 55-2011) [48], the mixture proportions for the RAC included cement (420 kg/m^3), sand

(561 kg/m³), natural coarse aggregate (569.3 kg/m³), recycled coarse aggregate (569.3 kg/m³), and water (205 kg/m³). Following the Standard for the Test Methods of Concrete Physical and Mechanical Properties (GB/T 50081-2019) [49], standard cube specimens were tested for static compressive strength, yielding a measured value of 40.12 MPa. Additionally, Q235B-grade steel tubes were used, and their mechanical properties were evaluated in accordance with code [50]. The test results are summarized in **Table 3**.

Table 2. Physical properties of RCA

Aggregate type	Grading (mm)	Water absorption(%)	Apparent density(kg/m^3)	Crushing index(%)	Mass ratio of residual mortar(%)
RCA	10-20	4.53	2689.44	9.45	37.69

Table 3. Material properties of steel plates

Material	Thin t/mm	Yield strength f_y /MPa	Tensile strength f_t/MPa	Elastic modulus E/MPa
Steel tube	4	312	446	2.02×10^5
Angle steel	4	342	419	1.93×10^5
Batten plate	4	325	406	2.05×10^5
Stiffening rib plate	10	393	462	1.92×10^5
Base	20	344	424	2.01×10^5
WSJ structural glue	-	-	33	2500

2.3. Loading device and loading system

The loading setup and procedures were designed [51]. After pre-damage and strengthening, the specimen was secured to the base using eight M30 high-strength bolts, while the base itself was anchored to the rigid floor with ground anchor bolts. The loading configuration is illustrated in **Fig. 2.**

To apply and maintain a constant axial load on the columns, a hydraulic jack was used. A hydraulic actuator with a stroke of ±150 mm delivered the horizontal cyclic load. The entire loading process was conducted under cyclic conditions, with control based on the interlayer displacement angle R(R = Δ/L, Δ is the horizontal displacement at the column top and L is the effective column height). Initially, a single cycle was performed at R= ±0.0025rad, ±0.005rad, ± 0.0075rad. Afterwards, the three cycles were performed at the R= ±0.01rad, ±0.02rad, ±0.03rad, ±0.04rad, ±0.05rad. The test was terminated when the horizontal cyclic load (ultimate load) dropped below 85% of the peak load or the specimen could no longer sustain the load. The loading system is depicted in **Fig. 3.**

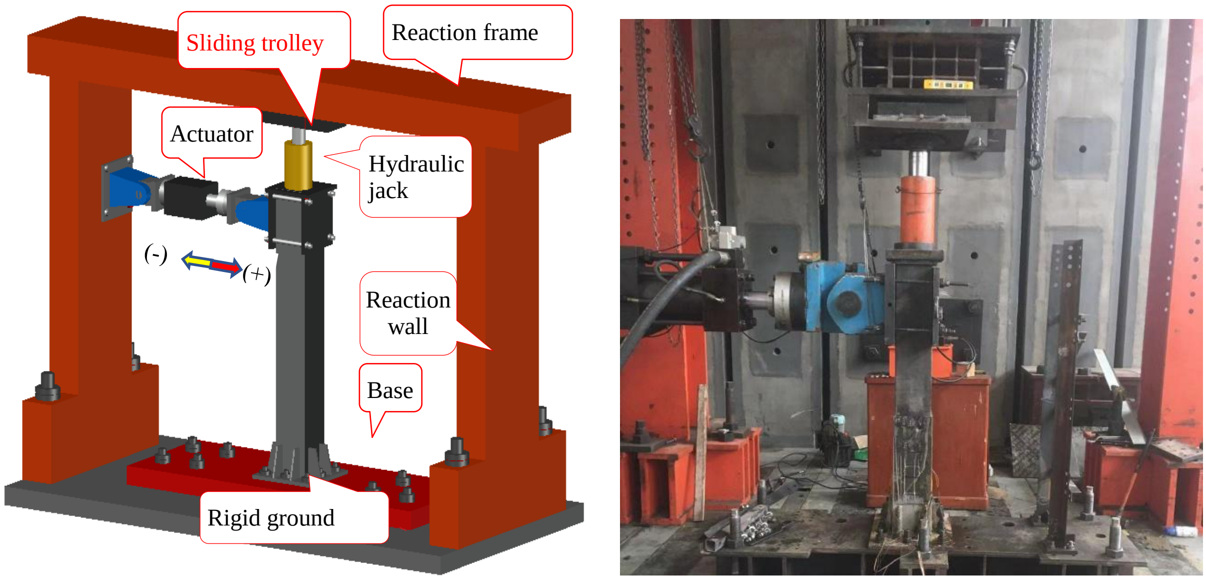

Fig. 2. Test loading device.

2.4. Test setup

During the experiment, strain gauges were utilized to measure the strain distribution on the specimens, with data recorded using a computer and strain meter. The gauges were positioned on both the front and back surfaces: gauges 1#, 2#, and 3# were attached to the front, while 4#, 5#, and 6# were placed on the back. The detailed layout of the strain gauges is illustrated in **Fig. 4.**

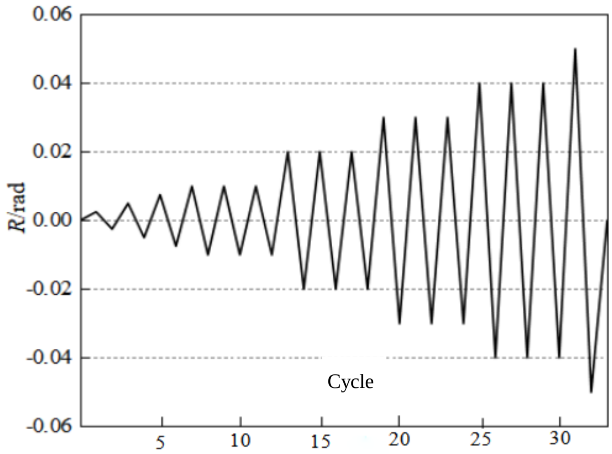

Fig. 3. Test loading system.

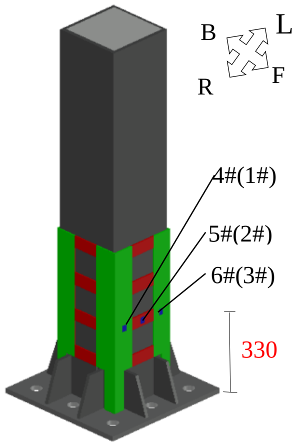

Fig. 4. Strain gauge of ESJ. (Unit: mm)

3. Description of the failure process

The positive direction corresponds to the actuator moving forward, while the negative direction indicates reversed loading. The side batten plates of the ESJ are numbered sequentially from top to bottom as 1, 2, 3, and 4.

The failure mode of specimen SEJS-0 is shown in **Fig. 5 (a)**. At R=±0.0075rad, the yield strain was happened. By the third cycle at R=±0.01rad, all strain gauges surpassed the yield strain. During the first cycle at R=±0.02rad, slight bulging appeared on the front and back sides, which recovered after unloading. By the third cycle at R=±0.03rad, the bulges became permanent, and slight bulging emerged on the two sides. At R=±0.04rad, irreversible elephant leg-like bulging occurred, and the horizontal load dropped below 85% of the peak load, leading to specimen failure.

The failure mode of specimen SEJS-1 is shown in **Fig. 5 (b)**. During the third cycle at R=±0.01rad, cracks formed at the ESJ-steel tube seal, accompanied by structural glue cracking sounds. At R=±0.02rad, all strain gauges exceeded the yield strain, and cracks expanded. By the third cycle at R=±0.02rad, slight bulging appeared between batten plates 3 and 4 on the front and back, which flattened under reverse loading. At R=±0.03rad, bulges enlarged, and cracks formed at the weld between batten plate 4 and angle steel on the left and right sides. By the third cycle at R=±0.03rad, cracks extended, and angle steel separated from the steel tube. At R=±0.04rad, bulges increased further, batten plate 4 tilted, and welds fractured, causing the horizontal load to drop below 85% of the peak load and resulting in specimen failure.

The failure mode of specimen SEJS-2 is shown in **Fig. 5 (c)**. Similar to SEJS-1, cracks appeared at the ESJ-steel tube seal during the third cycle at R=±0.01rad. At R=±0.02rad, all strain gauges exceeded the yield strain, and cracks expanded. By the third cycle at R=±0.02rad, slight bulging occurred between batten plates 3 and 4. At R=±0.03rad, bulges became permanent, and cracks formed at the weld between batten plate 4 and angle steel. By the third cycle at R=±0.03rad, cracks extended, and angle steel separated from the steel tube. At R=±0.04rad, batten plate 4 detached on the front side, and cracks expanded further, leading to specimen failure as the horizontal load dropped below 85% of the peak load.

The failure mode of specimen SEJS-3 is shown in **Fig. 5 (d).** Cracks appeared at the ESJ-steel tube seal during the third cycle at R=±0.01rad. At R=±0.02rad, all strain gauges exceeded the yield strain, and slight bulging occurred between batten plates 3 and 4. At R=±0.03rad, bulges enlarged, and cracks formed at the weld between batten plate 4 and angle steel. By the second cycle at R=±0.03rad, cracks extended to batten plate 2. At R=±0.04rad, cracks expanded further, and ESJ deformation increased, causing the horizontal load to drop below 85% of the peak load and resulting in specimen failure.

(a) SEJS-0 (b) SEJS-1 (c) SEJS-2 (d) SEJS-3

Fig. 5. Damage pattern of specimen.

Compared to the original specimen, the ESJ-strengthened specimens exhibited reduced bulging and no elephant leg-like deformation. Failure in these specimens primarily occurred at the welds between the angle steel and batten plates. For SEJS-1, cracks in the ESJ were mainly concentrated at the weld connecting the column base and the 4# batten plate. In contrast, SEJS-2 and SEJS-3 displayed wider cracks in the ESJ, which extended further upward.

4. Experimental results and analysis

4.1. Hysteretic loop curve

The hysteresis curves for specimens SEJS-0 to SEJS-3 are illustrated in **Fig. 6.** The yield load (p_y), ultimate load (P_m), and failure load (P_u) are denoted by black solid triangles, black solid pentagrams, and black solid squares, respectively. At storey drift angles (R) below 0.01 rad, all specimens remained in the elastic stage, exhibiting a nearly linear load-displacement relationship. Once R reached 0.01 rad, the specimens entered the elastic-plastic stage, surpassing their yield points. Failure occurred when R exceeded 0.04 rad.

All hysteresis curves displayed a full, shuttle-like shape without any pinching effect. This behavior is attributed to the confinement provided by the ESJ and steel tube, which placed the RCA under triaxial compression. The pre-damage and RCA defects did not induce pinching in the curves.

Compared to SEJS-0, the ultimate load capacities of SEJS-1, SEJS-2, and SEJS-3 increased by 29.9%, 26.3%, and 6.4%, respectively. The hysteresis curves of the strengthened specimens were fuller, with larger loop areas, demonstrating that the ESJ enhanced load capacity, ductility, and energy dissipation. Additionally, the seismic performance of the strengthened columns not only recovered but also surpassed their pre-damage levels.

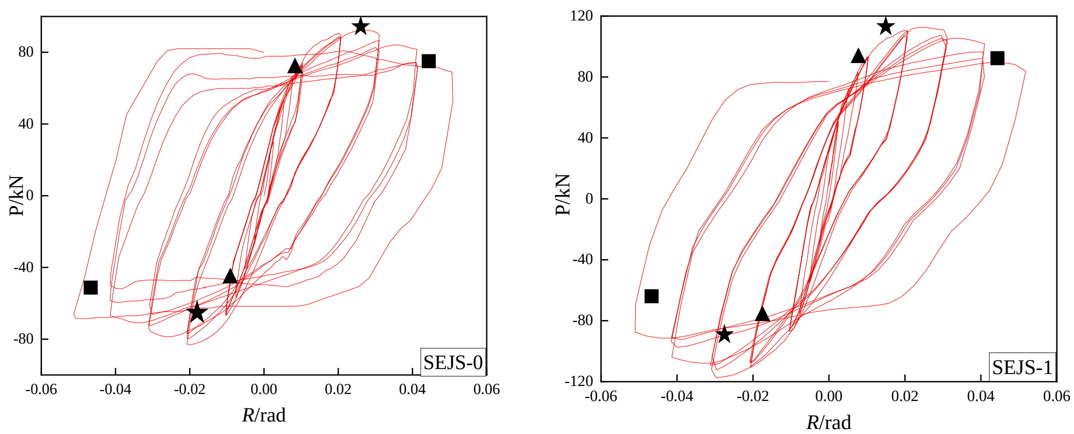

(a) SEJS-0 (b) SEJS-1

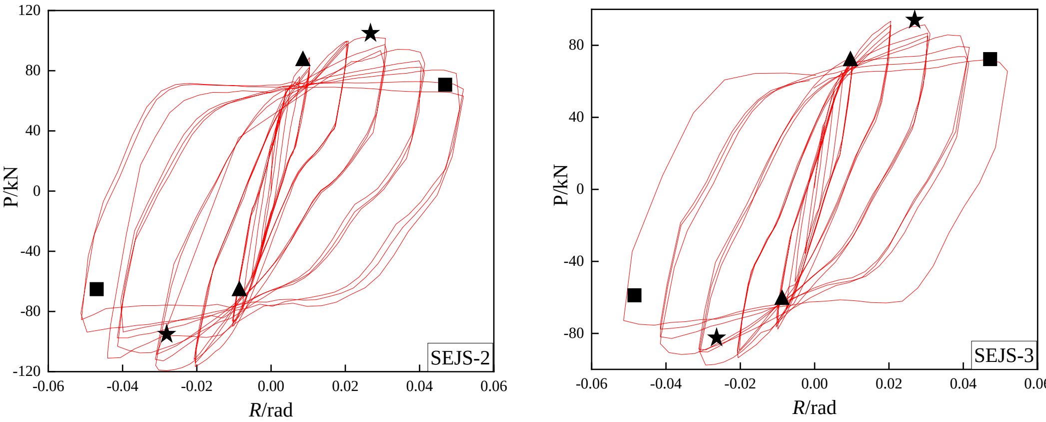

(c) SEJS-2 (d) SEJS-3

Fig. 6. Hysteresis curves.

4.2. Skeleton curve

The skeleton curves are shown in **Fig. 7.** Initially, the strengthened specimens exhibited steeper slopes compared to SEJS-0, indicating that the ESJ contributed to stress distribution early in the loading process and enhanced initial stiffness. For undamaged and moderately damaged specimens, the ESJ significantly improved initial stiffness due to its effective reinforcement. However, this improvement was less pronounced in severely damaged specimens.

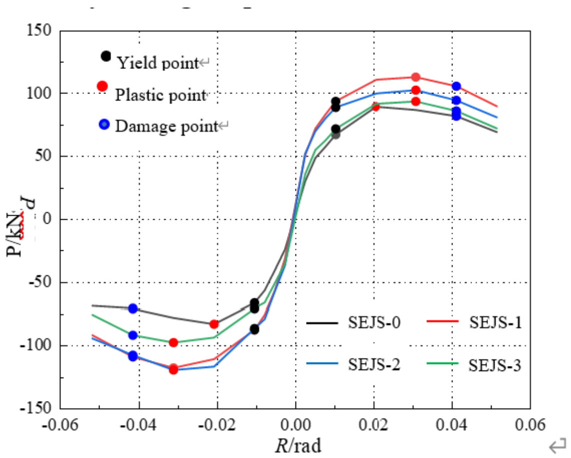

Fig. 7. Skeleton curves.

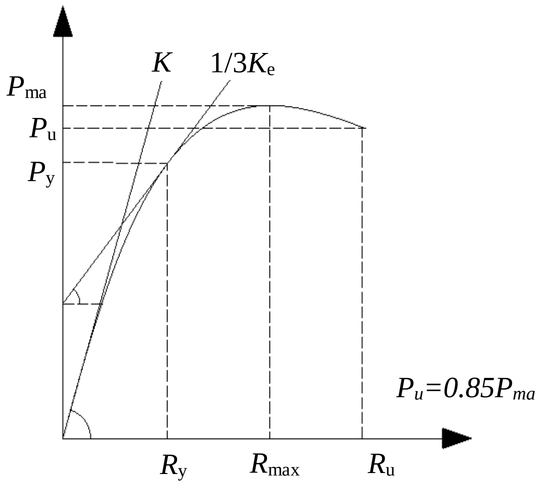

Fig. 8. The slope factor method.

4.3. Ductility analysis

Ductility, which reflects the plastic deformation capacity of structural components, significantly influences their seismic performance. The displacement ductility coefficient is defined as $\mu=R\text{u}/R\text{y}$, where Ru is the failure storey drift angle and Ry is the yield storey drift angle. In this study, the slope factor method [52] was used to identify the characteristic points of the specimens (see **Fig. 8**). The Ry was determined as one-third of the initial stiffness (*K*e), with the corresponding load designated as the yield load (*P*y). Additionally, Rm represents the maximum storey drift angle, Pmax denotes the ultimate load, Ru signifies the failure storey drift angle, and Pu indicates the failure load. **Table 4** summarizes the key characteristic points.

The ductility coefficients of the ESJ-strengthened specimens were higher than those of the unstrengthened control specimen (SEJS-0), demonstrating that the ESJ effectively enhanced ductility. Compared to SEJS-0, the ductility coefficients of SEJS-1, SEJS-2, and SEJS-3 increased by 29.2%, 26.4%, and 7.9%, respectively. Notably, the degree of ductility improvement was inversely related to the level of pre-damage.

Table 4. Load and displacement of the specimen at the characteristic point

Specimen	Loading direction	Yield point		Extreme point		Failure point		μ	μ improvement rate/%	*P*max improvement rate/%
		*P*y /kN	*R*y /rad	*P*max /kN	*R*max 、/rad	*P*u /kN	*R*u /rad			
SEJS-0	positive	73.6	0.0103	92.5	0.0203	78.6	0.0373	3.52	-	-
	negative	67.5	0.0102	83.2	0.0200	70.7	0.0348			
	average	70.6	0.0103	87.9	0.0202	74.7	0.0361			
SEJS-1	positive	93.5	0.0112	110.8	0.0303	94.2	0.0479	4.55	29.2	29.9
	negative	87.1	0.0112	117.6	0.0297	100.0	0.0461			
	average	90.3	0.0103	114.2	0.0300	97.1	0.0470			
SEJS-2	positive	93.6	0.0108	102.4	0.0268	87.0	0.0446	4.45	26.4	26.3
	negative	87.6	0.0112	119.5	0.0283	101.6	0.0459			
	average	90.6	0.0102	111.0	0.0276	94.3	0.0453			
SEJS-3	positive	73.5	0.0103	93.6	0.0207	79.6	0.0388	3.80	7.9	6.4
	negative	74.5	0.0102	93.3	0.0207	79.3	0.0390			
	average	74.0	0.0103	93.5	0.0207	79.5	0.0389			

4.4. Energy dissipation capability analysis

The energy dissipation capacity is quantified by the area enclosed within the hysteresis loop. Two metrics, the energy dissipation coefficient (E) and the equivalent viscous damping coefficient (h_e), are used to assess this capacity. As illustrated in **Fig. 9**, E_1 represents the area enclosed by the hysteresis loop ABCD, while E_2 corresponds to the combined areas of triangles OBE and ODF. The formulas for calculating E and h_e are as follows:

$$E_p = E_1 / E_2 \tag{5}$$

$$h_e = E / (2\pi) \tag{6}$$

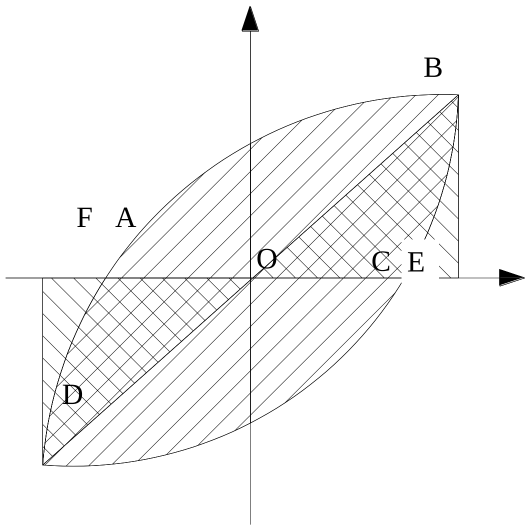

Fig. 9. Diagram of energy dissipation coefficient *E*.

The E and h_e for each specimen at various loading stages are presented in **Fig. 10**. As depicted, both E and h_e exhibited a continuous increase across all specimens. Additionally, these coefficients for the strengthened specimens showed an inverse relationship with the degree of pre-damage.

Compared to the original specimen, the energy dissipation capacity of the ESI-strengthened specimens improved significantly. During the yield stage, the E and h_e values of the strengthened specimens exceeded those of SEJS-0, demonstrating that the ESJ contributed to energy absorption and deformation at this stage. At this point, the energy dissipation coefficients of the strengthened specimens were nearly identical, suggesting that pre-damage had minimal impact on their energy dissipation performance. In the peak and failure stages, the E and h_e values of the ESJ-strengthened specimens remained higher than those of SEJS-0, indicating that the energy dissipation capacity of RACFRST columns, regardless of pre-damage levels, could recover or even surpass their original performance after ESJ strengthening.

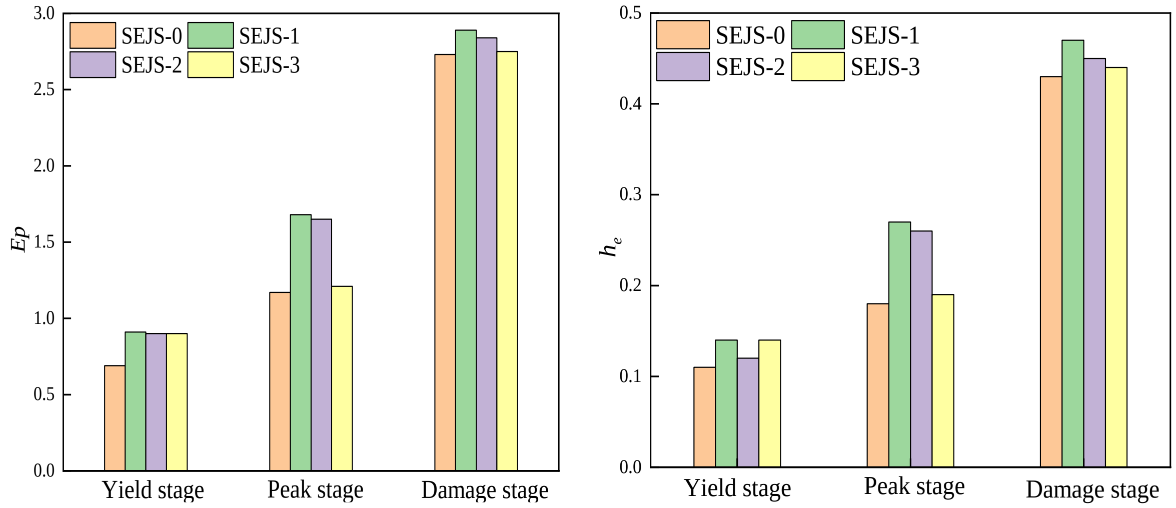

(a) Total energy dissipation (b) Equivalent viscous damping coefficient

Fig. 10. Different stages of total energy dissipation and equivalent viscous damping coefficient.

4.5. Bearing capacity degradation

To evaluate the degradation of bearing capacity, the bearing capacity degradation coefficient (λ_i) was introduced. This coefficient is defined as the ratio of the maximum horizontal load in the third cycle to that in the first cycle under each displacement level. The calculation formula is provided in Eq. (7), and the degradation curve is illustrated in **Fig. 11.**

$$\lambda_i = P_{3,i} / P_{1,i} \tag{7}$$

where $P_{3,i}$ represent the peak load of the third cycle at the ith loading displacement respectively; $P_{1,i}$ represent the peak load of the first cycle at the ith loading displacement.

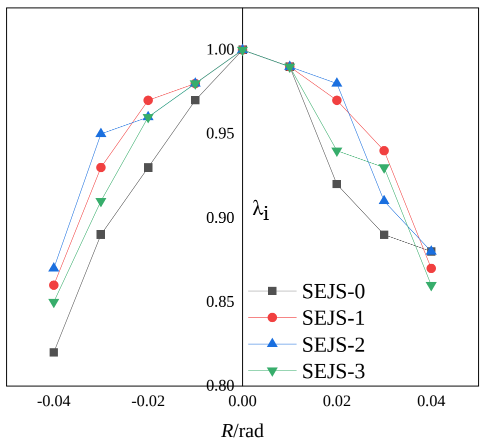

Fig. 11. Load bearing curves.

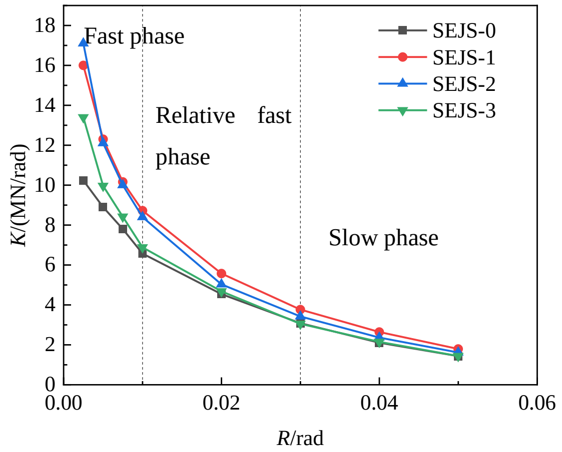

Fig. 12. Stiffness degradation curves.

Compared to the unstrengthened control specimen, the strengthened specimens exhibited higher λ_i values, demonstrating that the ESJ effectively delayed the degradation of load-bearing capacity. Additionally, the strengthened specimens showed fluctuations during the degradation process, attributed to the ESJ's energy absorption, which slowed the formation of plastic hinges and the subsequent decline in capacity. In the later loading stages, these fluctuations diminished as the ESJ sustained damage in the plastic-hinge region, reducing its confinement effect and causing a rapid decrease in bearing capacity.

4.6. Stiffness degradation

The overall stiffness degradation of the specimens is described by quoting the secant stiffness (K_i). Secant stiffness calculation formula is shown in Eq (8). **Fig. 12** shows the stiffness degradation curves of each specimen.

$$K_i = \sum_{i=1}^{3} P_{ij} / \sum_{i=1}^{3} R_{ij} \tag{8}$$

where P_{ij} represents the maximum loading force of the i-th cycle at the j-th stage; and the R_{1j} represents the interlayer displacement angle of the i-th cycle at the j-th stage.

As the storey drift angle increased, the secant stiffness of all specimens progressively declined. Initially, stiffness decreased rapidly, followed by a slower reduction phase. The degradation process for all specimens transitioned through rapid, moderately rapid, and slow stages. The strengthened specimens exhibited higher secant stiffness compared to SEJS-0, demonstrating that the ESJ effectively delayed stiffness degradation, with the extent of delay inversely related to the degree of pre-damage. During pre-damage, the steel tube and RAC in the plastic-hinge region of SEJS-3 experienced more severe damage than in SEJS-1 and SEJS-2, leading to distinct stiffness degradation curves. However, the ESJ had minimal impact on delaying stiffness degradation in severely damaged specimens.

4.7. Strain analysis

Since strain changes in the elastic stage were negligible, strain analysis focused on the yield, peak, and failure stages. **Fig. 13** illustrates the strain curves for each specimen at these stages, highlighting their variations.

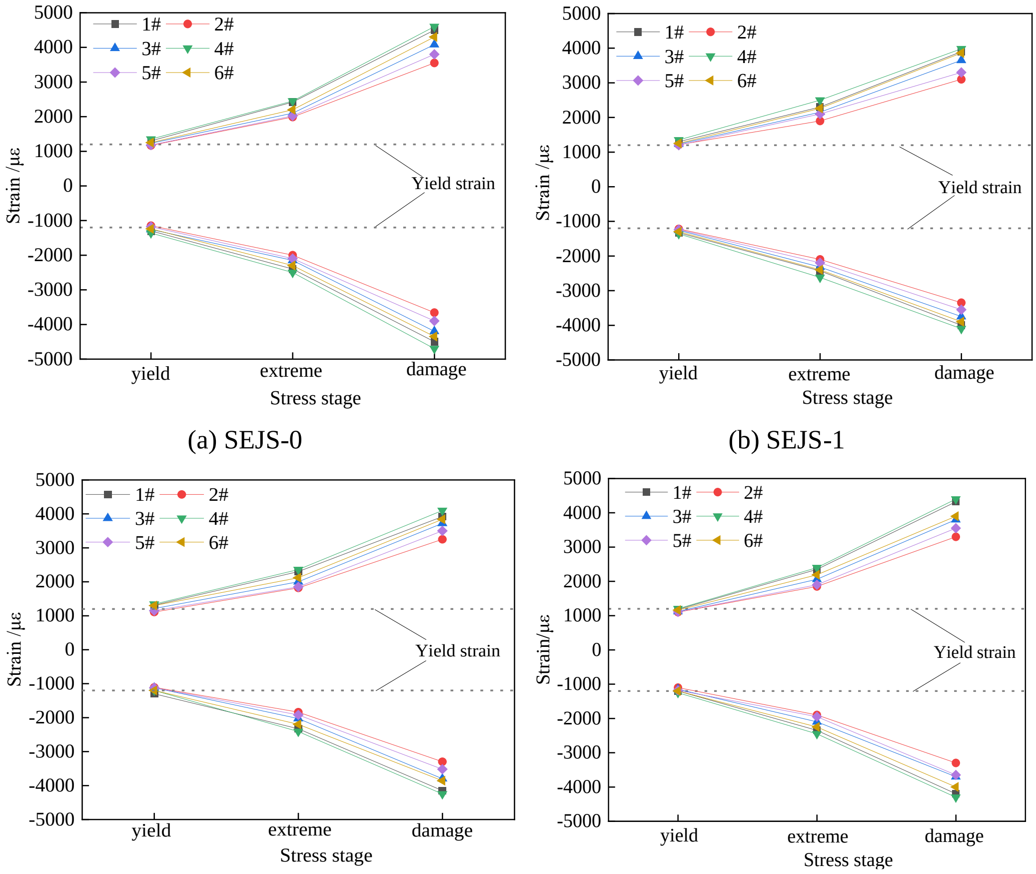

(a) SEJS-0 (b) SEJS-1

(c) SEJS-2 (d) SEJS-3

Fig. 13. Strain in each stage of specimen.

The confinement provided by the ESJ and steel tube restrained bulging and RAC crushing, resulting in relatively flat strain curves for SEJS-1 to SEJS-3. Across all stages, the strain values of ESJ-strengthened specimens were lower than those of SEJS-0, indicating that the ESJ participated throughout the loading process and effectively suppressed deformation. At failure, the strain values followed the order: SEJS-1 < SEJS-2 < SEJS-3, showing that failure deformation increased with pre-damage severity, though not linearly. Comparing SEJS-3 and SEJS-1, their strain values and trends were similar, with SEJS-3 slightly higher. This suggests that ESJ strengthening can partially restore load-bearing capacity lost due to seismic damage, but its effectiveness is limited and cannot fundamentally alter the component's failure mode. Enhancing the seismic performance of such components requires improvements in structural design.

5. Seismic capacity evaluation of ESJ-strengthened seismic-damaged RACFRST columns

According to the above experimental result, it could be found that the seismic capacity of seismic-damaged RACFRST columns was significantly degraded after earthquake. Although the ESJ strengthening could compensate for the loss of seismic capacity to a certain extent, it is extremely difficult to grasp and describe the degree of remediation. Currently, the normalized seismic damage model, which incorporates maximum deformation and cumulative energy dissipation, is widely used to assess the seismic performance of structural components. Among these, the Park-Ang model is particularly prevalent, with its formula provided in Eq. (9) [53].

$$D = \frac{\delta_m}{\delta_u} + \beta \frac{E_h}{f_y \delta_u} \tag{9}$$

where δ_m is the maximum deformation of the member under reciprocating load; δ_u is the ultimate deformation under monotonic load; β is the energy dissipation factor of the member; f_y is the yield strength of the structure or member; and E_h is the total energy consumed by member from loading to destruction. The calculation formula of energy dissipation factor is:

$$\beta = \left(-0.447 + 0.073\lambda + 0.24n + 0.314\rho_l\right) \times 0.7^{\rho_w} \tag{10}$$

where n is the axial compression ratio; λ is shear span ratio of the member; ρ_l is the longitudinal steel reinforcement ratio; ρ_w is the volume hoop ratio of the member.

While Eqs. (9) and (10) are commonly applied to calculate the seismic damage index for RC structures, the model has limitations in its boundary conditions and lacks in-depth consideration of seismic damage severity and the confining effect of steel tubes in plastic hinge regions. To address these issues, the boundary conditions were refined, and an energy dissipation factor was introduced, accounting for seismic damage levels and the confining effect of the steel tube. This factor is crucial for evaluating the seismic capacity of ESJ-strengthened, seismically damaged RACFRST columns. The modified Park-Ang model and its energy dissipation factor are expressed as follows:

$$D = \left(1-\beta\right) \frac{\delta_m}{\delta_u} + \beta \frac{E_h}{f_y \left(\delta_u - \delta_y\right)} \tag{11}$$

$$\beta = \left(-0.447 + 0.073\lambda + 0.24n + 0.314\rho_l + \alpha D_I + C\right) \times 0.7^{\rho_w} \tag{12}$$

where δ_y is the yield deformation of specimen under monotonic loading; α is the influence coefficient of the pre-damaged degree; D_I is the interlayer displacement angle corresponding to the pre-damaged degree; C is a constant; other parameters have the same meaning as the parameters in Eq (9) and Eq (10).

Inevitably, the seismic action will lead to the hooping effect in the plastic hinge area of RACFRST columns. The acquisition of the longitudinal binding force (ρ_l) and the circumferential binding force (ρ_W) in this region is the prerequisite for determining the parameters of Eq (11) and Eq (12). According to the equivalent action, the following calculation formula could be obtained.

Seismic actions inevitably induce a confining effect in the plastic hinge regions of RACFRST columns. Determining the longitudinal (ρ_l) and circumferential (ρ_W) binding forces in this area is essential for calculating the parameters in Eqs. (11) and (12). Based on the principle of equivalent action, the following formulas were derived:

$$\rho_l = \frac{f_{yl} A_s}{\frac{\pi}{4} f_y \left(d-2t\right)^2} \tag{13}$$

$$\rho_w = \frac{f_{wh} A_s}{\frac{\pi}{4} f_y \left(d-2t\right)^2} \tag{14}$$

where ρ_l and ρ_W represent the longitudinal and circumferential binding forces of the steel tube, respectively; f_y is the yield strength of steel tube; A_s and A_c are the area of steel tube and area of core concrete; d is the edge length; t is the wall thickness. f_{yl} and f_{wh} are the longitudinal stress and circumferential stress in the plastic hinge region of the damaged RACFRST column under earthquake, respectively, which are calculated by Eqs (15)~(18).

$$f_0 = \begin{cases} \left[1+\left(-0.054\xi^2+0.4\xi\right)\left(24/f_c\right)^{0.45}\right] f_c \\ \left(-1.254+2.254\sqrt{1+7.94\, f_r/f_c}-2\, f_r/f_c\right) \end{cases} \tag{15}$$

where f_0 is the ultimate compressive strength; f_r is the lateral pressure, as shown in Eq (16); ξ is the confining coefficient, as shown in Eq (17); f_c is axial compressive strength of concrete.

$$f_r = 2tf_{wh} / (d-2t) \tag{16}$$

$$\xi = A_s f_y / (A_c f_c) \tag{17}$$

From simultaneous Eqs (15) to (17), the following relationship is obtained:

$$f_{yl}^2 + f_{wh}^2 - f_{yl} f_{wh} = f_y^2 \tag{18}$$

The seismic damage index (D) at the time of failure in Eq (11) is equal to 1.0, and the specific value of the energy dissipation factor (β) is inversely calculated, as shown in **Table 5.**

Table.5 Experimental values of energy dissipation factor calculated by modified Park-Ang model

Loading direction	SEJS-1	SEJS-2	SEJS-3
Positive	0.025	0.023	0.021
Negative	0.018	0.020	0.018

To determine the specific values of the unknown parameters in Eq (12), the data in **Table 3** were substituted into Eq (12) by the method of undetermined coefficients. Therefore, the calculation formula of energy dissipation factor that considers pre-damaged degrees and steel tube's hooping effect is as follows:

$$\beta = \left(-0.447+0.073\lambda+0.24n+0.314\rho_l-0.09D_I-0.045\right)\times 0.7^{\rho_w} \tag{19}$$

To further study the application of Eq (12) in Eq (11), the experimental data were substituted into Eq (11) and Eq (12), and the seismic damage indexes of specimens SEJS-1~SEJS-3 were calculated as 0.965, 0.980 and 1.002, respectively. As shown by the result, the established seismic damage model of ESJ-strengthened RACFRST columns is feasible and can be used to quantitatively evaluate the seismic capacity of such components.

6. Conclusion

The effectiveness of ESJ in strengthening seismically damaged RACFRST columns was investigated through horizontal cyclic loading tests. The following conclusions were drawn:

(1) The failure patterns of RACFRST columns under cyclic loading resembled those of RACFST columns, with elephant leg-like bulging in the plastic hinge region. However, the ESJ confined bulging to the area between its bottom plates, preventing severe deformation. The ESJ significantly delayed the onset and progression of bulging.

(2) Compared to the control specimen, ESJ-strengthened specimens exhibited higher ultimate load capacities and greater ultimate strains.

(3) The ultimate load capacities increased by 25.4%, 25.0%, and 6.2%, while ductility indices rose by 25.7%, 20.0%, and 5.7%, respectively. The strengthening effect diminished with increasing seismic damage severity.

(4) Considering the influence of pre-damage severity and the steel tube's confining effect, regression analysis was performed on the energy dissipation factor (β) and pre-damage levels. A mathematical expression for β was derived, and the modified Park-Ang model's damage index at failure approached 1.0, accurately reflecting the damage behavior of ESJ-strengthened RACFRST columns.

Acknowledgement

This research is funded by National Natural Science Foundation of China (Grant No. 51678457), Natural Science Foundation of Hubei Province (Grant No. 2022CFB662), State Key Laboratory of Precision Blasting and Hubei Key Laboratory of Blasting Engineering of China (Grant No. PBSKL2022D05), Wuhan Knowledge Innovation Special Dawn Plan Project of China (Grant No. 2023020201020403) and their support is gratefully acknowledged.

CRediT authorship contribution statement

Sheng Peng: Investigation, Formal analysis, Writing–original draft. **Huangkai Sun:** Conceptualization, Funding acquisition, Supervision, Investigation, Formal analysis, Writing–original draft. **Ben Mou:** Supervision, Writing–review & editing. **Dongping Wu and Xianqi Xie:** Supervision, Investigation.

Conflicts of Interest

The authors declare that they have no conflicts of interest to report regarding the present study.

Data Availability Statement

Some or all data, models, or codes that support the findings of this study are available from the corresponding author upon reasonable request.

References

[1] Sadati S, Arezoumandi M, Khayat KH, Volz JS. Shear performance of reinforced concrete beams incorporating recycled concrete aggregate and high-volume fly ash. Journal of Cleaner Production 2016; 115: 284-293. https://doi:10.1016/j.jclepro.2015.12.017.

[2] Xu YJ, Chen HN, Liang YH, Shen J, Yang HX. Study on fracture characteristics and fracture mechanism of fully recycled aggregate concrete using AE and DIC techniques. Construction and Building Materials 2024; 419: 135540. https://doi.org/10.1016/j.conbuildmat.2024.135540.

[3] Li ZW, Li LY, Cheng SS. Evaluation of modulus of elasticity of concrete containing both natural and recycled concrete aggregates. Journal of Cleaner Production 2024; 447: 141591. https://doi.org/10.1016/j.jclepro.2024. 141591.

[4] Xu L, Chen J, Chen YH, Luo CS, Syed HYB. Cyclic performance of recycled aggregate with ferronickel slag concrete-filled steel tube columns. Structures 2024; 60: 105947. https://doi.org/10.1016/j.istruc.2024.105947.

[5] Ren QF, Pacheco J, Brito DJ, Hu JH. Analysis of the influence of the attached mortar's geometry on the mechanical behaviour of recycled aggregate concrete through mesoscale modelling. Engineering Fracture Mechanics 2024; 297: 109876. https://doi.org/10.1016/j.engfracmech.2024.109876.
Hamed D, Mahdi K, Ali K, Amirreza K, Farid S. Compressive strength of concrete with recycled aggregate; a machine learning-based evaluation. Cleaner Materials 2022; 3: 100044. https://doi:10.1016/J.CLEM A.2022. 100044.

[6] Tang YX, Xiao JZ, Zhang HH, Duan ZH, Xia B. Mechanical properties and uniaxial compressive stress-strain behavior of fully recycled aggregate concrete. Construction and Building Materials 2022; 323: 126546. https://doi:10.1016/J.CONBUILDMAT.2022.126546.

[7] Fernanda AS, Flávio AS. Recycled aggregates from construction and demolition waste towards an application on structural concrete: A review. Journal of Building Engineering 2022; 52: 104452. https://doi:

10.1016/J.JOBE.2022.104452
[8] Yu XF, Yao QF, Wang GL, Li YZ. Mechanical characteristics and analyses of seismic performance of multi-rib slab wall. Journal of Xi'an University of Architecture and Technology (Natural Science Edition) 2009; (6): 827-833. https://doi:10.3969/j.issn.1006-7930.2009.06.016.
[9] Grabiec AM, Zawal D, Rasaq WA. The Effect of Curing Conditions on Selected Properties of Recycled Aggregate Concrete. Applied Sciences 2020; 10(4441): 4441-4451. https://doi:10.3390/app10134441.
[10] Jang YH, Choi KS, You YC, Kim KH, Yun HD. Effect of recycled coarse aggregate (RCA) replacement level on the bond behaviour between RCA concrete and deformed rebars. Journal of the Korea Concrete Institute 2010; 22(1):123-130. https://doi:10.4334/JKCI.2010.22.1.123.
[11] Hamad BS, Dawi AH. Sustainable normal and high strength recycled aggregate concretes using crushed tested cylinders as coarse aggregates. Case Studies in Construction Materials 2017; 7: 228-239. https://doi:10.1016/j. cscm.2017.08.006.
[12] Zhang HH, Xiao JZ, Tang YX, Duan ZH, Poon CS. Long-term shrinkage and mechanical properties of fully recycled aggregate concrete:Testing and modelling. Cement and Concrete Composites 2022; 130: 104527. https:// doi:10.1016/J.CEMCONCOMP.2022.104527.
[13] Alberto DC, Carlos L, Fernando LG, Miguel ASL, Pedro SJO. Castaño T. Creep and shrinkage of recycled aggregate concrete. Construction and Building Materials 2009; 23(7): 2545-2553. https://doi:10.1016/j. conbuildmat.2009.02.018.
[14] Han LH, Li W, Bjorhovde R. Developments and advanced applications of concrete-filled steel tubular (CFST) structures: Members. Journal of Constructional Steel Research 2014; 100: 211-228. https://doi:10.1016/j. jcsr.2014.04.016.
[15] Tu CL, Shi YJ, Liu D, Wang WH, Ban HY. Behavior and general design method of concrete-filled high-strength steel tube (CFHST) columns. Engineering Structures 2021; 243: 112506. https://doi:10.1016/J. ENGSTRUCT.2021.112506.
[16] Peng S, Xiong Z. Experimental study on the seismic behavior of CFRP-strengthened seismic-damaged recycled aggregate concrete-filled rectangular steel tube frame columns. Journal of Building Engineering 2022; 45: 103422. https://doi:10.1016/J.JOBE.2021.103422.
[17] Zhang XG, Gao X. The hysteretic behavior of recycled aggregate concrete-filled square steel tube columns. Engineering Structures 2019; 198(C): 109-523. https:// doi:10.1016/j.engstruct.2019.109523.
[18] Chen ZP, Xu JJ, Chen YL, Lui EM. Recycling and reuse of construction and demolition waste in concrete-filled steel tubes: A review. Construction and Building Materials 2016; 126: 641-660. https://doi:10.1016/j. conbuildmat.2016.09.063.
[19] Yang DD, Liu FQ, Wang YY. Axial compression behaviour of rectangular recycled aggregate concrete-filled steel tubular stub columns. Journal of Constructional Steel Research 2023; 201: 107687. https://doi.org/10.1016/j.j csr.2022.107687.
[20] Zhao PT, Huang Y, Liu ZZ, Wang H, Lu YY. Experimental research on seismic performance of steel fiber-reinforced recycled concrete-filled circular steel tube columns. Journal of Building Engineering 2022; 54: 104683. https://doi:10.1016/J.JOBE.2022.104683.
[21] Shi XS, Wang QY, Zhao XL, Collins FG. Structural behaviour of geopolymeric recycled concrete filled steel tubular columns under axial loading. Construction and Building Materials 2015; 81: 187-197. https://doi:10.1016/j.conbuildmat.2015.02.035.
[22] Wang YY, Chen J, Geng Y. Testing and analysis of axially loaded normal-strength recycled aggregate concrete filled steel tubular stub columns. Engineering Structures 2015; 86: 192-212. https://doi:10.1016/j. engstruct.2015.01.007.
[23] Yang YF, Fu F, Bie XM. Behaviour of rectangular RACFST slender columns under eccentric compression. Journal of Building Engineering 2021; 38: 102236. https://doi:10.1016/J.JOBE.2021.102236.
[24] Chen LH, Pouyan F, Danial ER, Mohammad HJ, Alireza MAA, Younes N. Axial compressive strength predictive models for recycled aggregate concrete filled circular steel tube columns using ANN, GEP, and MLR [J]. Journal of Building Engineering,2023,77: 107439. https://doi.org/10.1016/j.jobe.2023.107439.
[25] Yang YB, Chen GL, Wu YX, Li XX, Li FL, Zhao SB. A case study on seismic behavior of circular-sectional steel tubular columns filled with concrete of 100% recycled aggregates. Case Studies in Construction Materials 2022; 16: e00992. https://doi.org/10.1016/j.cscm.2022.e00992.
[26] Luo CS, Wang FX, Chen HY, Qi A, Chen Y. Study on the hysteretic behavior of recycled aggregate concrete-filled steel tube columns containing ferronickel slag. Journal of Building Engineering 2022; 46: 103695. https://doi:10.1016/J.JOBE.2021.103695.
[27] Dong HY, Qin J, Chen Z, Cao WL, Tang YP. Seismic behavior of full-scale square high-strength RACFST columns. Structures 2021; 34: 2600-2616. https://doi:10.1016/J.ISTRUC.2021.09.031.
[28] Thanoon WA, Jaafar MS, Kadir MRA, Noorzaei J. Repair and structural performance of initially cracked reinforced concrete slabs. Construction and Building Materials 2005; 19(8): 595-603. https://doi:10.1016/j. conbuildmat.2005.01.011.

[29] Wei C, Shao YB, Chen C, Mohamed HS. Axial compressive strength of preloaded CHS stubs strengthened by CFRP. Marine Structures 2022; 84: 103242. https://doi:10.1016/J.MARSTRUC.2022.103242.

[30] Zhang JG, Wu B, Mei Y, Shing PB. Experimental and analytical studies on a reinforced concrete frame retrofitted with buckling-restrained brace and steel caging. Advances in Structural Engineering 2015; 18(2): 155-171. https://doi:10.1260/1369-4332.18.2.155.

[31] Abdulrahman S, Hussein E, Husain A, Tarek A, Yousef AS. Behavior of axially loaded L-shaped RC columns strengthened using steel jacketing. Journal of Building Engineering 2022; 47: 103870. https://doi:10. 1016/J.JOBE.2021.103870.

[32] Abdulrahman S, Hussein E, Husain A, et al. Behavior of axially loaded L-shaped RC columns strengthened using steel jacketing. Journal of Building Engineering 2022; 47: 103870. https://doi.org/10.1016/j.jobe. 2021. 103870.

[33] Saadi RI, Hussein AA. Behavior of RC columns strengthened by combined (CFRP and steel jacket). Materials Today: Proceedings 2022; 61(P3): 1126-1134. https://doi.org/10.1016/j.matpr.2021.10.514.

[34] Liu J, Xue YT, Wang CK, Nie JG, Wu ZH. Experimental investigation on seismic performance of mechanical joints with bolted flange plate for precast concrete column. Engineering Structures 2020; 216(C): 110729. https://doi:10.1016/j.engstruct.2020.110729.

[35] Kwan AKH, Dong CX, Ho JCM. Axial and lateral stress-strain model for circular concrete-filled steel tubes with external steel confinement. Engineering Structures 2016; 117: 528-541. https://doi: 10.1016/j. engstruct.2016.03.026.

[36] Lai M.H, Ho JCM. Axial strengthening of thin-walled concrete-filled-steel-tube columns by circular steel jackets. Thin-Walled Structures 2015; 97: 11-21. https://doi:10.1016/j.tws.2015.09.002.

[37] Zhang D, Li N, Li ZX, Xie LL. Experimental investigation and confinement model of composite confined concrete using steel jacket and prestressed steel hoop. Construction and Building Materials 2020; 256(C): 119399. https://doi:10.1016/j.conbuildmat.2020.119399.

[38] Zha XF, Lu MX, Yang B, Zhao B. Experimental study on CFSST columns strengthened by enveloped steel under low cycle reversed loading. Journal of Yangtze University (Nature Science Edition) 2015; 12(34): 42-47. https://doi:10.16772/j.cnki.1673-1409.2015.34.014.

[39] Xu CX, Yang B, Lu MX, Zha XF. Comparative experimental study on strengthening approach of seismic-damaged CFSST columns. Journal of Guangxi University (Nature Science Edition) 2016; 41(1): 53-62. https://doi:10.13624/j.cnki.issn.1001-7445.2016.0053.

[40] GB 50936-2014, Technical code for concrete filled steel tubular structures. Beijing: China Architecture & Building Press, 2014.

[41] Wu B, Zhao XY, Zhang JS. Cyclic behavior of thin-walled square steel tubular columns filled with demolished concrete lumps and fresh concrete. Journal of Constructional Steel Research 2012; 77: 69-81. https://doi.org/10.1016/j.jcsr.2012.05.003.

[42] GB 50011-2010, Code for seismic design of buildings. Beijing: Ministry of Housing and Urban-Rural Development of the People's Republic of China, 2010.

[43] GB 50017-2017, Standard for design of steel structures. Beijing: China Architecture & Building Press, 2017.

[44] Xu CX, Peng S, Wang F, Ma ZT. Influence of the degree of damage and confinement materials on the seismic behavior of RC beam-SRC column composite joints. Composite Structures 2020; 231: 111002. https:// doi:10. 1016/j.compstruct.2019.111002.

[45] GB 50550-2010, Code for acceptance of construction quality of strengthening building structures. Beijing: China Architecture & Building Press, 2010.

[46] Yang YF, Han LH. Experimental behaviour of recycled aggregate concrete filled steel tubular columns. Journal of Constructional Steel Research 2006; 62(12): 1310-1324. https://doi:10.1016/j.jcsr.2006.02.010.

[47] JGJ 55-2011, Specification for mix proportion design of ordinary concrete. Beijing: China Architecture & Building Press, 2011.

[48] GB/T 50081-2019, Standard for test methods of concrete physical and mechanical properties. Beijing: China Architecture & Building Press, 2019.

[49] GB/T 228.1-2010, Metallic materials-Tensile testing-Part 1: Method of test at room temperature. Beijing: General Administration of Quality Supervision, Inspection and Quarantine of the People's Republic of China; Standardization Administration of China,2010.

[50] JGJ/T 101-2015, Specification for seismic test of buildings. Beijing: Ministry of Housing and Urban-Rural Development of the People's Republic of China, 2015.

[51] Mou B, Li X, Bai YT, Wang LS. Shear behavior of panel zones in steel beam-to-column connections with unequal depth of outer annular stiffener. Journal of Structural Engineering 2019; 145(2): 04018247. https://doi:10.1061/(ASCE)ST.1943-541X.0002256.

[52] Park YI, Ang HS. Mechanistic seismic damage model for reinforced concrete. Journal of Structure Engineering ASCE 1985; 111(4): 722-739.